JOURNAL OF
Applied Polymer
SCIENCE

Special Issue: Polymers for Microelectronics

Guest Editors: Dr Brian Knapp (Promerus LLC) and
Prof. Paul A. Kohl (Georgia Institute of Technology)

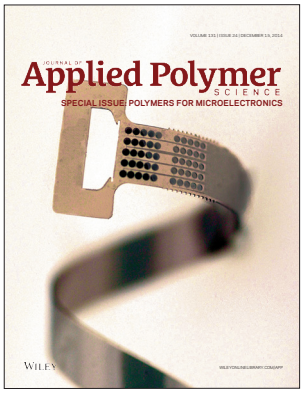

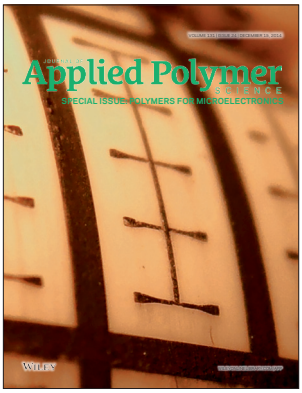

EDITORIAL

Polymers for Microelectronics
B. Knapp and P. A. Kohl, *J. Appl. Polym. Sci.* 2014, **DOI: 10.1002/app.41233**

REVIEW

Negative differential conductance materials for flexible electronics
A. Nogaret, *J. Appl. Polym. Sci.* 2014, **DOI: 10.1002/app.40169**

RESEARCH ARTICLES

Generic roll-to-roll compatible method for insolubilizing and stabilizing conjugated active layers based on low energy electron irradiation
M. Helgesen, J. E. Carlé, J. Helt-Hansen, A. Miller, and F. C. Krebs, *J. Appl. Polym. Sci.* 2014, **DOI: 10.1002/app.40795**

Selective etching of polylactic acid in poly(styrene)-block-poly(D,L)lactide diblock copolymer for nanoscale patterning
C. Cummins, P. Mokarian-Tabari, J. D. Holmes, and M. A. Morris, *J. Appl. Polym. Sci.* 2014, **DOI: 10.1002/app.40798**

Preparation and dielectric behavior of polyvinylidene fluoride composite filled with modified graphite nanoplatelet
P. Xie, Y. Li, and J. Qiu, *J. Appl. Polym. Sci.* 2014, **DOI: 10.1002/app.40229**

Design of a nanostructured electromagnetic polyaniline–Keggin iron–clay composite modified electrochemical sensor for the nanomolar detection of ascorbic acid
R. V. Lilly, S. J. Devaki, R. K. Narayanan, and N. K. Sadanandhan, *J. Appl. Polym. Sci.* 2014, **DOI: 10.1002/app.40936**

Synthesis and characterization of novel phosphorous-silicone-nitrogen flame retardant and evaluation of its flame retardancy for epoxy thermosets
Z.-S. Li, J.-G. Liu, T. Song, D.-X. Shen, and S.-Y. Yang, *J. Appl. Polym. Sci.* 2014, **DOI: 10.1002/app.40412**

Electrical percolation behavior and electromagnetic shielding effectiveness of polyimide nanocomposites filled with carbon nanofibers
L. Nayak, T. K. Chaki, and D. Khastgir, *J. Appl. Polym. Sci.* 2014, **DOI: 10.1002/app.40914**

Morphological influence of carbon modifiers on the electromagnetic shielding of their linear low density polyethylene composites
B. S. Villacorta and A. A. Ogale, *J. Appl. Polym. Sci.* 2014, **DOI: 10.1002/app.41055**

Electrical and EMI shielding characterization of multiwalled carbon nanotube/polystyrene composites
V. K. Sachdev, S. Bhattacharya, K. Patel, S. K. Sharma, N. C. Mehra, and R. P. Tandon, *J. Appl. Polym. Sci.* 2014, **DOI: 10.1002/app.40201**

Anomalous water absorption by microelectronic encapsulants due to hygrothermal-induced degradation
M. van Soestbergen and A. Mavinkurve, *J. Appl. Polym. Sci.* 2014, **DOI: 10.1002/app.41192**

Design of cyanate ester/azomethine/ZrO_2 nanocomposites high-k dielectric materials by single step sol-gel approach
M. Ariraman, R. Sasi Kumar and M. Alagar, *J. Appl. Polym. Sci.* 2014, **DOI: 10.1002/app.41097**

Furan/imide Diels–Alder polymers as dielectric materials
R. G. Lorenzini and G. A. Sotzing, *J. Appl. Polym. Sci.* 2014, **DOI: 10.1002/app.40179**

High dielectric constant polyimide derived from 5,5'-bis[(4-amino) phenoxy]-2,2'-bipyrimidine
X. Peng, Q. Wu, S. Jiang, M. Hanif, S. Chen, and H. Hou, *J. Appl. Polym. Sci.* 2014, **DOI: 10.1002/app.40828**

The influence of rigid and flexible monomers on the physical-chemical properties of polyimides
T. F. da Conceição and M. I. Felisberti, *J. Appl. Polym. Sci.* 2014, **DOI: 10.1002/app.40351**

JOURNAL OF
Applied Polymer
SCIENCE

Special Issue: Polymers for Microelectronics

Guest Editors: Dr Brian Knapp (Promerus LLC) and
Prof. Paul A. Kohl (Georgia Institute of Technology)

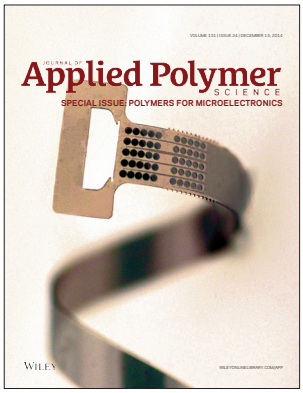

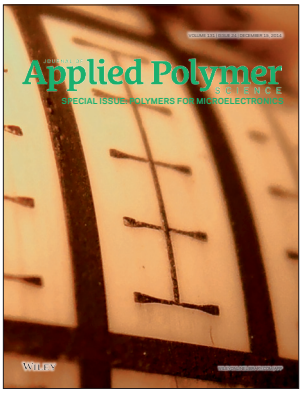

Development of polynorbornene as a structural material for microfluidics and flexible BioMEMS
A. E. Hess-Dunning, R. L. Smith, and C. A. Zorman, *J. Appl. Polym. Sci.* 2014, **DOI:** 10.1002/app.40969

A thin film encapsulation layer fabricated via initiated chemical vapor deposition and atomic layer deposition
B. J. Kim, D. H. Kim, S. Y. Kang, S. D. Ahn, and S. G. Im, *J. Appl. Polym. Sci.* 2014, **DOI:** 10.1002/app.40974

Surface relief gratings induced by pulsed laser irradiation in low glass-transition temperature azopolysiloxanes
V. Damian, E. Resmerita, I. Stoica, C. Ibanescu, L. Sacarescu, L. Rocha, and N. Hurduc, *J. Appl. Polym. Sci.* 2014, **DOI:** 10.1002/app.41015

Polymer-based route to ferroelectric lead strontium titanate thin films
M. Benkler, J. Hobmaier, U. Gleißner, A. Medesi, D. Hertkorn, and T. Hanemann, *J. Appl. Polym. Sci.* 2014, **DOI:** 10.1002/app.40901

The influence of dispersants that contain polyethylene oxide groups on the electrical resistivity of silver paste
T. H. Chiang, Y.-F. Chen, Y. C. Lin, and E. Y. Chen, *J. Appl. Polym. Sci.* 2014, **DOI:** 10.1002/app.41183

Quantitative investigation of the adhesion strength between an SU-8 photoresist and a metal substrate by scratch tests
X. Zhang, L. Du, and M. Zhao, *J. Appl. Polym. Sci.* 2014, **DOI:** 10.1002/app.41108

Thermodynamic and kinetic aspects of defectivity in directed self-assembly of cylinder-forming diblock copolymers in laterally confining thin channels
B. Kim, N. Laachi, K. T. Delaney, M. Carilli, E. J. Kramer, and G. H. Fredrickson, *J. Appl. Polym. Sci.* 2014, **DOI:** 10.1002/app.40790

Journal of Applied Polymer Science

Design of a Nanostructured Electromagnetic Polyaniline–Keggin Iron–Clay Composite Modified Electrochemical Sensor for the Nanomolar Detection of Ascorbic Acid

Reena Viswan Lilly, Sudha Janardhanan Devaki, Rohini Kuttiplavil Narayanan, Neethu Kalloor Sadanandhan

National Institute of Interdisciplinary Science and Technology, Thiruvananthapuram 695019, India

Correspondence to: S. J. Devaki (E-mail: sudhajd2001@yahoo.co.in)

ABSTRACT: This article demonstrates the design and fabrication of an electrochemical sensor based on a platinum electrode for ascorbic acid (AA) modified by an electromagnetic polyaniline–Keggin iron–clay (PPICS) composite. The polyaniline–polyhydroxy iron–clay composite was prepared by the polymerization of $[Anilinium]^+[PDPSA]^-$ in the presence of Keggin iron intercalated clay and was characterized for its particle size, morphology, electrical conductivity, and saturation magnetization. The oxidation potential of AA was observed at +0.4 V on the bare electrode and shifted to a negative potential of −0.32 V on the modified electrode. Common possible interferences of the sample matrices were tested, and the results reveal that the PPICS-modified electrode exhibited a high selectivity and sensitivity toward AA. This unique low-cost and user-friendly sensor was validated for the nanomolar detection of AA present in real samples. © 2014 Wiley Periodicals, Inc. J. Appl. Polym. Sci. **2014**, *131*, 40936.

KEYWORDS: clay; conducting polymers; electrochemistry; emulsion polymerization; magnetism and magnetic properties

Received 25 February 2014; accepted 30 April 2014

DOI: 10.1002/app.40936

INTRODUCTION

Conducting polymers (CPs) are superior functional materials because of their extended π conjugation, reversible doping–dedoping process, and unique conduction mechanism. They possess excellent processability, low cost, and light weight; these make them amenable for applications such as field-effect transistors, integrated circuits, batteries, sensors, supercapacitors, and energy storage devices. Nanostructured CPs have attracted significant attention because of their better performance, which is a result of their high electrical conductivity, large surface area, high electron charge, and mobility.[1–5] Because of the current inadequacy of strategies for nanofabrication, nanostructured CPs are now under development even in the area of nanoelectronic devices. The literature shows that with nanoimprint lithography, various kinds of nanostructures, such as dots, wires, and optical gratings, have been fabricated. Chi et al.[6] prepared large-area nanowire arrays of CP nanocomposites using nanoimprint lithography. They demonstrated its advantages in device fabrication by giving electrical connection to suitably sized metal electrodes and used them as electrochemical nanosensors with a high error tolerance in the device performance. Eftekhari[7] provided an imperative link between nanotechnology and conductive polymers and studied magnetic particle-incorporated CPs for electrochemical sensor applications. Among nanostructured CPs, polyaniline (PANI) has been widely employed in chemical and biosensor development because of its good stability, ease of preparation, conductivity, pH, and redox sensitivity.[8,9] PANI can be synthesized by several strategies, including controlled solution synthesis, soft-template methods, hard-template synthesis, electrospinning, and nanoscale lithography. There have been several reports in the literature on the synthesis of nanostructured PANIs with chemical oxidative polymerization and their electrochemical-sensing applications.[10–14] Nanostructured CPs immobilized with redox materials have attracted considerable research attention as electrochemical sensors because of their excellent sensitivity via enhanced interaction between CP and analytes.

Smectite clays are interesting inorganic layered hosts for the preparation of functional materials because of their small particle size, capacity for swelling, and exchange cations for intercalation.[15] They have thin layers of aluminum silicate that organize to form stacks with a regular van der Waal's gap between them called *interlayer spacing* or a *gallery*. The presence of exchangeable cations in the galleries and the variability of the

Additional Supporting Information may be found in the online version of this article.

© 2014 Wiley Periodicals, Inc.

c-axis dimension permit the intercalation of a large variety of inorganic and organic cations, and desirable physical properties can be engineered into these materials.[16] Bradley and Kydd[17] reported the intercalation of polyhydroxy iron cation {PIC; $[FeO_4Fe_{12}(OH)_{24}(H_2O)_{12}]^{7+}$} into smectite clay and studied its utility as a selective catalyst. PIC is a polycondensation product obtained during the acidic hydrolysis of ferric chloride. These cations have discrete structures of definite sizes and shapes belonging to the well-known structural Keggin type. They find catalytic applications because of their easily accessible Fe^{2+}/Fe^{3+} redox couple and large number of unpaired electrons in high spin combined with the possibility formation for the spin–crossover magnetic molecular materials.[18] Earlier, we reported the preparation of a conducting PANI–Keggin iron–clay composite.[19] The limitation of that system was the difficulty we had in getting stable dispersions because of the large surface area of the PIC particles.[20] Block copolymers and surfactants have been reported as stabilizing agents for controlling the size and shape of nanoparticles by capping mechanism.[21] We also observed the formation of nanostructured/microstructured PANI and PANI–clay nanocomposites with amphiphilic dopants developed from cashew nut shell liquid, which played the multiple roles of micellar template, structure-directing agent, dopant, intercalating agent, and more.[22–25] Earlier, our group prepared a polyaniline–Keggin iron–clay (PPICS) composite using 3-pentadecyl phenol-4-sulfonic acid (3-PDPSA) as an amphiphilic dopant and blended it with polycarbonate for electromagnetic interference shielding applications.[26] In this article, we demonstrate the design and performance characteristics of a PPICS-modified electrode with respect to its sensitivity, operational stability, and storage life for the sensing of L-ascorbic acid (AA).

AA, better known as vitamin C, is one of the most important biological compounds; it takes part in several significant biological processes, such as immune response, wound healing, therapeutic processes, and animal metabolism. It is a powerful antioxidant and is present in food and beverages. It is also a marker chemical for the evaluation of food deterioration and product quality. Furthermore, AA has been an object of increasing interest in the cosmetic industry for antiaging treatments.[27] In view of these several functionalities, the estimation of AA has attracted a great deal of attention in the biomedical engineering, food, and pharmaceutical industries.[28]

Electrochemical methods for the estimation of AA have been greatly preferred during recent years because of their simplicity, accuracy, reproducibility, and specificity for various chemical species. They are also adaptable to even small sample volumes.[29] Matos et al.[30] measured AA in beers, soda, natural juices, and commercial vitamin C tablets with a palladium-modified gold electrode. However, the main drawback in this approach was the high overpotential for AA oxidation, in which many electroactive substances usually present in real samples could also get oxidized and interfere in the detection. One of the most common ways to overcome this problem is the use of modifiers that allow direct electron transfer between the active site and the electrode surface.[31] Among the various mediator-modified electrodes, CP-modified electrodes have been widely used for the immobilization of mediators.[32,33] These electrodes have exhibited a good stability and catalytic effects that result from their three-dimensional mediator distribution. This approach, although it exhibits good sensitivity and accuracy, suffers from some important shortcomings, including a high cost, low stability, and limited binding to solid surfaces. For this reason, during the last decade, enzymes have been preferred as electrochemical inorganic mediators,[34] which catalyze the oxidation of AA. This results in a decrease in the applied potential and the consequent prevention of much electrochemical interference. An ascorbic sensor based on a molecularly imprinted polymer modified hanging mercury electrode and an AA-imprinted, polymer-modified graphite electrode was reported by Prasad et al.[35] A Prussian blue (PB) modified electrode system was used by researchers for the oxidation of AA.[36] They studied the electrochemical catalytic activity of Fe^{2+}/Fe^{3+} present in PB by depositing PB layers onto different electrode materials (e.g., platinum, glassy carbon, SnO_2, TiO_2). However, all of these modifiers suffer from high cost and low storage stability.

In this context, the combination of the catalytic efficiency and redox properties of Fe^{2+}/Fe^{3+} in PIC, the excellent electrical conductivity of nanostructured PANI, and the enhanced electron-transfer rate process facilitated by nanoclay layers was used in the design of an electrochemical sensor based on water-dispersible nanostructured multifunctional PPICS as a novel system for an AA assay. The conventional sensor materials used in the electrode modification for the sensing of AA were metal nanoparticles, poly(Nile blue), PB dyes, carbon nanotubes, graphene, and so forth. In this study, electrode modification was performed with PPICS. PPICS was made from three low-cost materials, as aniline, clay, and Keggin iron, and the amphiphilic surfactant, PDPSA, was derived from a low-cost and abundantly available renewable resource based on cardanol (20 rupees/1 kg). The derivatization process of cardanol with sulfuric acid, isolation, and its purification was also very simple. Keggin iron was prepared by the simple acidic hydrolysis of ferric chloride. Here, we report a low-cost PPICS nanocomposite as a sensor for the nanomolar detection of AA. Common possible interference of the sample matrices were also tested to confirm the electrode's selectivity for AA and also applied for the analysis of AA present in real samples, such as vitamin C tablets.

EXPERIMENTAL

Reagents

Aniline (99.5% pure) was distilled under reduced pressure. Sodium carbonate, glucose, fructose, tartaric acid, and resorcinol were purchased from Ranbaxy Fine Chemicals, Ltd. Ammonium persulfate (APS), methanol, and ferric chloride hexahydrate were purchased from S. D. Fine Chem, Ltd. (Mumbai, India). Na^+ Cloisite clay, with a cation exchange capacity of 92.6 mequiv/100 g, was purchased from Loba Chemie (Bombay, India). 3-PDPSA was prepared from 3-pentadecyl phenol (cardanol), which was obtained by the double distillation of cashew nut shell liquid (Cashew Export Promotion Council, India) at 3–4 mmHg at 230–235°C. AA was purchased from SRL, India. All chemicals were analytical grade and were used without further purification. Fresh sample solutions were used for each experiment. 3-PDPSA and PIC were prepared as reported elsewhere.[20,25]

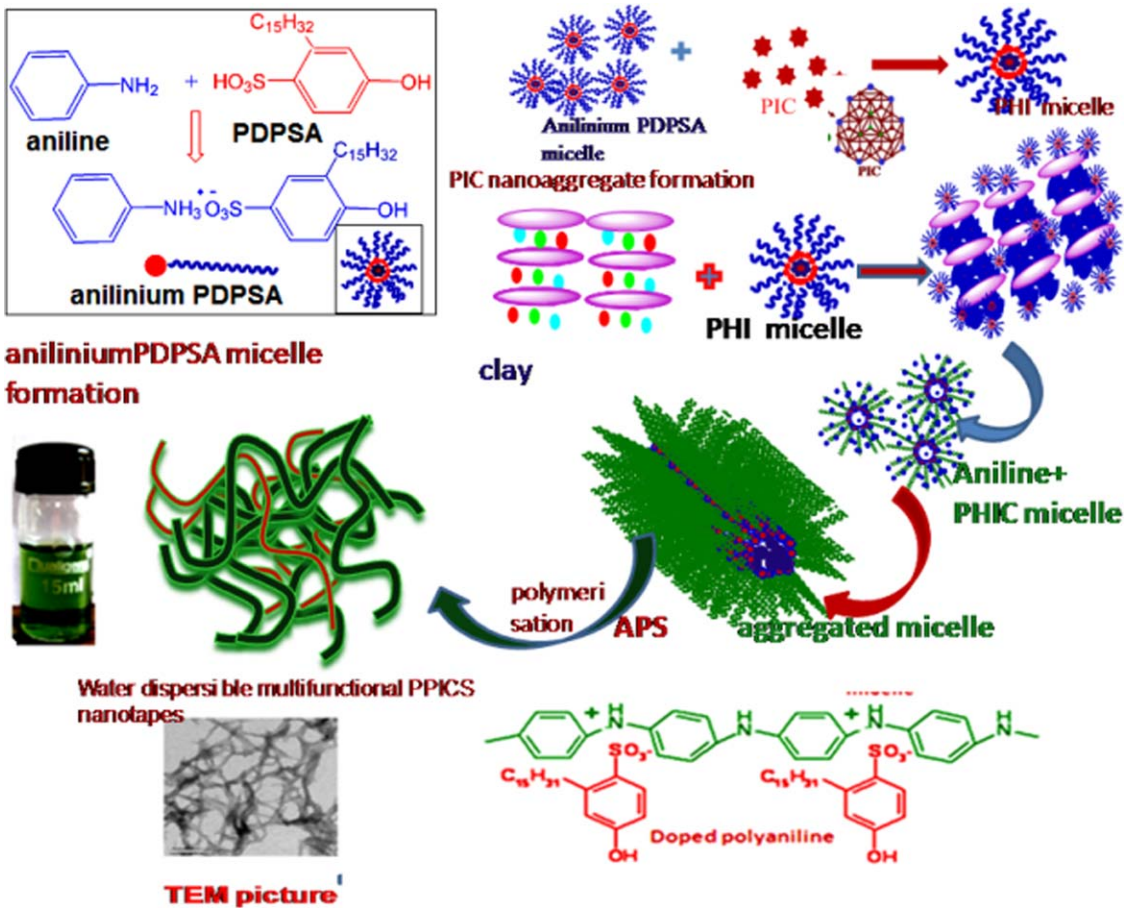

Scheme 1. Schematic representation of the preparation of the water-dispersible nanostructured PPICS. PHI, polyhydroxy iron cation. [Color figure can be viewed in the online issue, which is available at wileyonlinelibrary.com.]

Preparation of PIC

PIC was prepared by the hydrolysis of ferric chloride hexahydrate, and the procedure is given in the Supporting Information (Scheme S1).[18]

Preparation of 3-PDPSA and Polyaniline–Polyhydroxy Iron–Clay (PPIC)

The preparation processes of 3-PDPSA and PPIC are provided in the Supporting Information.

Preparation of the Multifunctional PPICS Composite

PPICS was synthesized by the reaction between PIC and aniline in the presence of the dopant 3-PDPSA. PPICS was prepared as per a previously reported procedure,[26] and the detailed synthetic procedure is given in the Supporting Information. Similarly, experiments were carried out with various ratios of PDPSA; these were designated as PPICS1, PPICS2, PPICS3, PPICS4, and PPICS5, respectively. For comparison, PANI, PANI and clay (PPC), and PANI and PIC (PPI) were prepared under similar conditions.

Construction of the PPICS Sensor

A Pt electrode was dipped in 50% HNO_3 overnight and washed thoroughly with doubly distilled water before use. It was polished to a mirror finish with alumina powder (0.05 μm) and ultrasonicated for 5 min. The Pt electrode (diameter = 3 mm, area = 28.26 mm^2) was modified by dipping in an aqueous PPICS dispersion (0.2*M*) overnight. All of the electrochemical experiments were carried out in a three-electrode cell with the PPICS/Pt modified electrode as a working electrode, a saturated Ag/AgCl electrode as the reference electrode, and platinum wire as the auxiliary electrode. The modified electrode was electroactivated by scanning in the potential range between −0.5 and 1 V in phosphate buffer solution (PBS, pH 7.0) with cyclic voltammetry (CV) at a scan rate of 50 mV/s. Before we performed the experiments, the solution was purged with nitrogen gas for 10 min. After the current achieved a steady state, the cyclic voltammograms were recorded by the addition of aliquots of the analyte into the cell. In all of the experiments for the estimation of AA, fresh solutions were prepared. Operational stability and storage life were also studied under the same experimental conditions.

Instruments

The ultraviolet–visible (UV–vis) absorption spectra were studied by the dispersion of the sample in deionized water, and we recorded the spectra using a UV–vis spectrophotometer (Shimadzu, model 2100) in the range 300–1100 nm. Fourier transform infrared (FTIR) measurements were made with a fully computerized Nicolet Impact 400D FTIR spectrophotometer. PPICS was mixed thoroughly with potassium bromide and

compressed into pellets before recording. All of the spectra were corrected for the presence of moisture and carbon dioxide in the optical path. The molecular weight was measured with a matrix-assisted laser desorption/ionization time of flight (MALDI-TOF) mass spectrometer (AXIMA CFR, Shimadzu) equipped with a nitrogen laser emitting at 337 nm and α-cyano-4-hydroxy cinnamic acid as the matrix. X-ray diffraction (XRD) studies were performed with an X-ray diffractometer (Philips X'Pert Pro) with Cu Kα radiation ($\lambda \approx 0.154$ nm) employing an X'celarator detector and a monochromator at the diffraction beam side. Powder samples were used with a standard sample holder. An averaged 2θ was used with a 2θ resolution of 0.002° from 2 to 70°. For conductivity measurements, the samples were pressed into a disk with a diameter of 13 mm, and they were measured with a standard four-probe method with a Keithley 6881 programmable current source and a 2128A nanovoltmeter at 30°C. The resistivity of the samples was measured at three different positions, and at least three pellets were measured for each sample: an average of nine readings was used for the conductivity calculations. For scanning electron microscopy measurements, the samples were subjected to thin gold coating with a JEOL JFC-1200 fine coater. The probing side was inserted into a JEOL JSM-5600 LV scanning electron microscope to take photographs. Transmission electron microscopy (TEM) was performed in an FEI TECNAI 30G2 S-TWIN microscope with an accelerating voltage of 100 kV. For TEM measurements, the water suspensions of the samples were fully dispersed under ultrasonication. Then, these were deposited onto a Formvar-coated copper grid and dried at room temperature before observation. Particle size measurement was done via a Nano ZS Malvern instrument with a 4-mW He–Ne laser ($\lambda = 632.8$ nm) equipped with a thermostated sample chamber. Magnetic property measurements were made with vibrating sample magnetometry. Powder samples were used to observe the hysteresis behavior of the nanoparticles at room temperature. All CV studies were performed in an electrochemical analyzer (CHI620B). The experiments were performed at ambient temperature in a one-compartment electrochemical cell with a three-electrode system.

RESULTS AND DISCUSSION

Preparation and Characterization of PPICS

The amphiphilic dopant, 3-PDPSA was prepared and characterized as per the procedure reported.[21] Aniline and 3-PDPSA formed salt because of the acid–base reaction between the —SO_3H groups of 3-PDPSA and the —NH_2 groups of aniline. Further, anilinium–PDPSA self-assembled to form micellar structures (Scheme 1). The solubility of anilinium–PDPSA in water was studied, and it was observed to form a stable emulsion in water. The critical micelle concentration of anilinium–PDPSA in water was determined by measurement of the intensity of scattered light with the dynamic light scattering (DLS) technique with various concentrations of 3-PDPSA ranging from 10^{-5} to $10^{-3}M$. PIC was prepared by the acidic hydrolysis of ferric salt. The formation of PIC $\{[FeO_4Fe_{12}(OH)_{24}(H_2O)_{12}]^{7+}$ (Keggin ion)$\}$ involved several steps, including hydrolysis, polycondensation, nucleation, and crystallization. These polycondensed particles aggregated to form PIC microparticles because of their high surface area and the magnetic dipole interactions among the PIC nanoparticles. In this study, PIC was stabilized with $10^{-4}M$ PDPSA. The effect of PDPSA in controlling the aggregation of PIC was envisaged by DLS measurement. In the absence of PDPSA, PIC exhibited highly aggregated polydispersed microparticles, whereas in the presence of 3-PDPSA, it showed monodispersed nanoparticles of 7.0 nm in size (PDI = 0.5; Figure S1, Supporting Information). Thus, the particle nucleation and growth mechanism could be controlled with the dopant, 3-PDPSA. In the presence of aniline, micelles of PIC-encapsulated anilinium–PDPSA were formed by an acid–base reaction. Later, they were intercalated inside the nanoclay layers by a cation-exchange process. The enhancement/displacement in the interlayer distance was evidenced from the XRD measurements. Thus, the aqueous solution contained micelles of self-assembled clay–PIC–anilinium–PDPSA. It was well accepted that the formed micelles were spherical in shape to minimize the surface energies.

It was reported that organic salts that contain a hydrophobic part and possess a charge opposite to that of the surfactant molecule are highly efficient in the promotion of a structural transition in micelles.[37] These cylindrical micelles may imbibe excess aniline molecules. Then, upon the addition of APS, polymerization proceeds, and this cylindrical micelle transforms into nanotapes by the process of elongation and flattening, as shown in Scheme 1. This has been supported by observations made by other researchers.[38] In this study,3-PDPSA played multiple roles as a micellar template, capping agent, dopant, and structure-directing agent during the formation of the PPICS nanotapes. The polymerized product was found to be dispersible in water and almost all organic solvents, including dichloromethane, chloroform, toluene, and tetrahydrofuran. The molecular weight of PPICS was measured with MALDI-TOF and showed values in the range of 40, 000 Da. DLS measurements showed the size of the particles as 70 nm, as shown in Figure S2 (Supporting Information).

UV–Vis Spectroscopy

The electronic state of the PPICS composites was studied by UV–vis spectroscopy. The UV–vis spectra of PANI, PPC, PPIC, and PPICS are shown in Figure S3 (Supporting Information). PANI exhibited three absorption peaks in the regions (1) about 340 nm (π–π^* transition), (2) about 420 nm (polaron band–π^* transition), and (3) about 700 nm (π–polaron band transition). In PPC, the peak at 430 nm was slightly flattened; this might have been due to the overlap with the π–π^* transition band at 350 nm, and thereby, this appeared as a single band and revealed a high level of doping.[39] Compared to PANI, the polaron band of PPC showed a redshift to 780 nm, which was due to the formation of delocalized charges in the polaron band promoted by the extended conformation of the PANI chains inside the clay galleries. The polaron band shifted to 810 and 830 nm in PPI and PPICS, respectively; this suggested more effective doping. The ratio of absorbance of the peaks [(π–polaron)/(π–π^*)] followed the order PPICS (1.13) > PPI (1.08) > PPC (1.0) > PANI (0.893); this suggested more effective doping in PPICS.

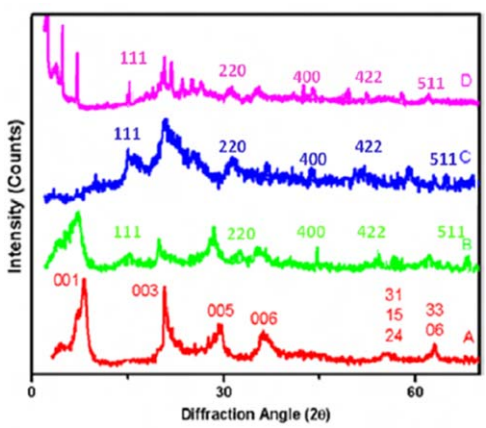

Figure 1. XRD diffractograms of (A) Na^+ Cloisite, (B) PHIC, (C) PPIC, and (D) PPICS. [Color figure can be viewed in the online issue, which is available at wileyonlinelibrary.com.]

FTIR Spectra

The FTIR spectra of PANI, PPI, and PPICS are shown in Figure S4(A–C) (Supporting Information), respectively. The absorption peak around 1574 and 1490 cm^{-1} were attributed to the C═C stretching of quinoid and benzenoid, respectively.[40] Generally, all of the spectra showed peaks at 1119 and 823 cm^{-1}, which were assigned to the aromatic in-plane bending vibrations of C—H, and the out-of-plane deformation of C—H in the 1,4-disubstituted benzene ring, respectively.[41] In PPICS, a prominent peak observed at 1030 cm^{-1} corresponded to the Si—O—Si structure of clay. The C═C stretching deformation of the quinoid in PANI shifted from 1580 to 1562 cm^{-1}, and that of the benzenoid ring shifted from 1503 to 1482 cm^{-1}; this indicated a longer effective delocalization in PPICS.[42–44] From a closer look at the spectra, we observed that the band at 1295 cm^{-1}, which was assigned as the stretching vibrations of C—N, shifted significantly to 1306 cm^{-1} in PPICS. This frequency shift of ν(C—N) observed in PPICS was believed to be caused by the hydrogen-bonding interactions between PANI and the basal surface of the clay (i.e., NH...O hydrogen bonding). The absorption bands around 630 cm^{-1} present in PPIC and PPICS were the characteristic bands of Fe—O stretching.[45] The bands at 1040 and 506 cm^{-1} were assigned to the absorption of the sulfonate group.[46] Interestingly, there were variations in the relative intensities and positions of the C═N and C═C stretching bands in PANI, PPI, and PPICS; this suggested that there could have been interactions between nitrogen sites in the PPI particles.[47]

XRD Studies

The wide-angle XRD patterns of Na^+ Cloisite, PIC and clay (PHIC), PPIC, and PPICS are shown in Figure 1(A–D), respectively. The diffraction pattern of clay showed reflections at $2\theta = 7.2°$ (d_{001}), 18.7° (d_{003}), 21.9° (d_{004}), 28.6° (d_{005}), 34.9° (d_{007}), 54.2° (d_{31}, d_{15},d_{24}), and 61.8° (d_{33}, d_{06}). The basal reflection peak at $2\theta = 7.2°$ with a d-spacing of 12.1 Å corresponded to the d_{001} basal spacing of the clay. In PHIC, the d_{001} reflection shifted to a lower angle with a d-spacing of 15 Å with an enhancement in the interlayer distance of 5.5 Å. The measured hike in the d-spacing was equal to the dimension of the hydrated PIC. The diffractogram exhibited additional reflections at $2\theta = 15°$ (111), 31° (220), 44.6° (400), 54.3° (422), 55° (422), and 65.1° (511); these were the characteristic peaks of the crystalline spinel structure of PIC.[48] The diffractogram of PPIC [Figure 1(C)] showed a silent reflection for the d_{001} peak of clay; this confirmed an exfoliated state in the nanoclay layers. In PPIC, the characteristic reflections were observed at $2\theta = 29.6°$ (3.01 Å), 35.29° (2.54 Å), 43.25° (2.09 Å), 54.1° (1.69 Å), and 61.97° (1.49 Å). In PPICS, the peaks were observed at $2\theta = 30.1°$ (2.97 Å), 35.42° (2.5 Å), 44.8° (2 Å), and 62.1° (1.5 Å). PPICS [Figure 1(D)] exhibited more intense extra peaks in the region $2\theta = 19°$; this revealed that there were more ordered crystalline PANI layers in the PPICS composite than in PPIC. Moreover, PPICS exhibited a sharp reflection below $2\theta = 5°$; this revealed the presence of a self-assembled PANI–PDPSA nanostructure in PPICS. The small discrepancy observed in the d values of iron oxide in PPIC and PPICSs compared to that of PIC may have been due to the partially collapsed phase of PIC in the presence of clay and the protonated PANI chains. Thus, it was reasonable to believe that a spinel structure of PIC, similar to that of the Fe_3O_4 present in PPICS, was responsible for the ferromagnetic properties exhibited by the PPICS composite.[49]

Morphology

The morphology of the samples was studied with TEM, and elemental analysis was performed by energy-dispersive spectrometry. The TEM pictures of PPICS1 and PPICS3 are shown in Figure 2(A,B), respectively. PPICS exhibited a tapelike morphology, with a diameter below 100 nm and extending to several micrometers in length, whereas PPIC exhibited an aggregated fiber morphology, as shown in the Supporting Information (Figure S5). The observed highly ordered nanotapes of PPICS were attributed to the formation of self-assembled PANI–PDPSA bilayer interactions. The dark region observed in the micrograph might have been due to the self-assembled magnetic PHIC particles, and the light region corresponded to the self-assembled PANI chains present in the composites. This contrast in the image might have arisen from the difference in the electron penetrability when it passed through the inorganic and organic moieties present both in the PPI and PPICS. The energy-dispersive spectrum of PPICS [Figure 2(C)] revealed the presence of elements such as carbon, sulfur, oxygen, and iron in PPICS.

Electrical Conductivity

The electrical conductivity of PPICS was measured with a four-probe conductivity meter. The conductivity of PPICSs was observed to be in the order PPICS5 (106 S/m) > PPICS4 (78 S/m) > PPICS3 (23 S/m) > PPICS2 (8.3 S/m) > PPICS1 (5.2 S/m); this suggested a decrease in the conductivity with decreasing PDPSA concentration. The conductivity of the inorganic–CP hybrid composites depended on the factors such as the doping level, conjugation, chain length, and some external factors, such as the compactness of the sample. Bulk PANI exhibited a conductivity of 3 S/m. The measured conductivity of PPICS was found to be two orders greater than that for bulk PANI (110 S/m). The possible explanation for the higher conductivity in PPICS was that during the polymerization process, the oligomeric species of aniline may have adsorbed magnetic PIC on

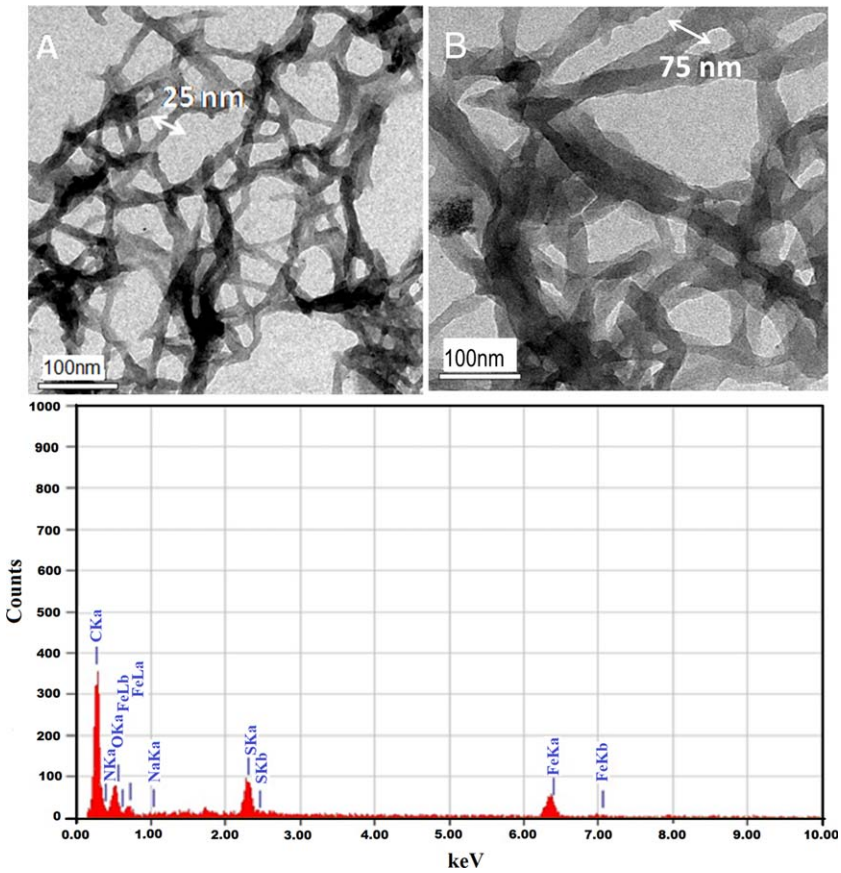

Figure 2. TEM images of (A) PPICS1 and (B) PPICS3 and (C) energy-dispersive X-ray spectroscopy image of PPICS3. CKa- Carbon Kα shell, NKa – Nitrogen Kα shell, OKa- Oxygen Kα shell, Fe Lb–Iron Lβ shell, Fe La- Iron Lα shell, Na Ka- sodium Kα shell, SKa–Sulfur Kα shell, SKb Sulfur Kβ shell, FeKa- iron Kα shell, Fe Kb- iron Kβ shell. [Color figure can be viewed in the online issue, which is available at wileyonlinelibrary.com.]

the surface. The crystalline boundaries became the primary nucleation centers, and these centers acted as structure-directing effects for the further propagation of PANI chains. Hence, the PPICS showed an increase in conductivity.

Magnetic Property Measurements

The magnetic properties of the nanostructured electromagnetic PPICSs were measured at room temperature with vibrating sample magnetometry. The magnetic properties measurement of CPs can provide information regarding the coercivity (H_C), remnant magnetization, and saturation magnetization (M_S). The hysteresis loop (M—H curve) showing M_S under an applied magnetic field of PPIC and PPICS is shown in Figure S6 (Supporting Information). PPICS5 exhibited an M_S of 10 emu/g and an H_C of 600 Oe. PPIC exhibited an M_S of 6 emu/g and an H_C of 530 Oe. Thus, the magnetic property measurement revealed direct evidence for the role of the dopants in controlling M_S and H_C. We observed that M_S increased with increasing dopant concentration; this may have been due to the increased number of charged species.[50,51]

CV Studies

The PPICS-modified Pt electrode was prepared as described in the Experimental section, and the cyclic voltammograms of PPICS were recorded in the potential range of − 0.5 to 1 V at a scan rate of 50 mV/s in PBS and are depicted in Figure S7 (Supporting Information). They exhibited two prominent peaks at 0.6 and −0.32 V. A report in the literature showed that PANI generally exhibits peaks around 0.8–0.6 and 0.2–0 V, which correspond to the conversion from the pernigraniline to the emeraldine state and from the emeraldine to the leucoemeraldine state, respectively.[52] The broad peak at 0.6 V observed for PPICS pertained to the oxidation of PPICS from the pernigraniline to the emeraldine state, and the broadness indicated a sluggish charge-transfer process during the oxidation.[53] The sharp peak at −0.32 V corresponded to the reduction of PPICS, preferably the Fe^{3+}/Fe^{2+} couple. The sharpness revealed its high rate of electron-transfer processing. The surface electron-transfer rate constant (K_S^o) and surface concentration ($Q\Gamma$) of the PPICS-modified Pt electrode was evaluated by experiments at different scan rates ranging from 20 to 200 mV/s. The effect of the potential scan rate (v) on the peak reduction current (I_p) is shown in Figure 3.

As expected, the peak current increased with increasing scan rate. The difference between the anodic potential and cathodic potential was observed to be 73 mV at 20 mV/s. With increasing scan rate, the cathodic potential shifted more toward the negative direction, and the anodic potential shifted toward the positive direction. This resulted in an increased ΔE_p (ΔE_p is the difference between cathodic potential and anodic potential); that is, the peaks departed from each other with an increase in the scan rate. The variation of ΔE_p as a function of the scan rate showed that the electron-transfer reaction at the electrode/solution interface was reversible.[54]

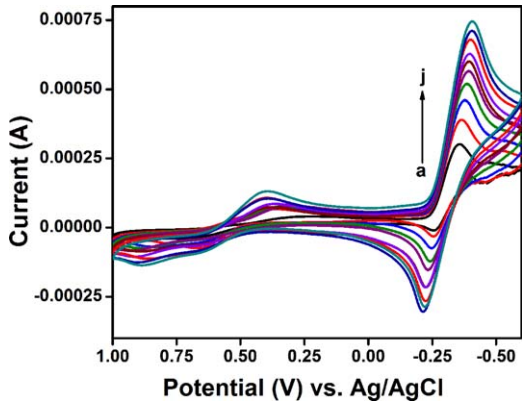

Figure 3. Cyclic voltammograms of the PPICS-modified Pt electrodes in PBS (pH 7) at different scan rates: (a) 20, (b) 40, (c) 60, (d) 80, (e) 100, (f) 120, (g) 140, (h) 160, (i) 180, and (j) 200 mV/s. [Color figure can be viewed in the online issue, which is available at wileyonlinelibrary.com.]

$Q\Gamma$ of PPICS was determined by the integration of the area under the cathodic peak. From the equation

$$I_p = \frac{n^2F^2\Gamma A v}{4RT}$$

where n is the number of electrons, A is the working electrode area (0.0707 cm^2), υ is the scan rate (20 mV/s), R is the universal gas constant, T is the absolute temperature, F is Faraday's Constant, Γ is the surface concentration, and $Q\Gamma = nFA\Gamma$, $Q\Gamma$ was calculated to be 6.9×10^{-8} mol/cm^2, which was far greater than reported values.[55,56]

PPICS-Modified Pt Electrode Based AA Sensor

The oxidation of AA at the bare electrode was irreversible and occurred at a high overpotential of 0.4 V. The nonreproducibility of the electrode response was due to the slow electron-transfer kinetics, which were presumably due to the fouling of the electrode surface by the oxidation product of AA at the bare electrode. Real analyte solutions, however, often contain plenty of oxidizable species other than ascorbate, which can also be oxidized anodically at a relatively high electrode potentials. Thus, the anodic current concerned with the electrooxidation of these substances could exceed the anodic current response concerned with the electrooxidation of ascorbate. So, it seemed to be of considerably great importance to create an electrocatalytically active electrode surface that could enable us to lower the electrooxidation potential of ascorbate to an appropriate level.

In general, PPICS transduces and amplifies the signal and increases the electrode's sensitivity to AA assay. The Pt/PPICS could detect AA at a lower potential of −0.32 V with a hike in the I_p intensity of the Fe^{3+}/Fe^{2+} couple. When AA was added to the solution, it catalyzed the electrochemical reduction of Fe^{3+} to Fe^{2+} and increased the peak current intensity proportionally when the AA concentration was increased. The schematic representation of the proposed electrode and its electrochemical reaction with AA is shown in Scheme 2. The increase in the oxidation current of AA may have been due to the favorable electrostatic attraction between the cationic PPICS and anionic AA. Such an interaction led to an increase in reactivity of AA within the electrode. The significant variation in

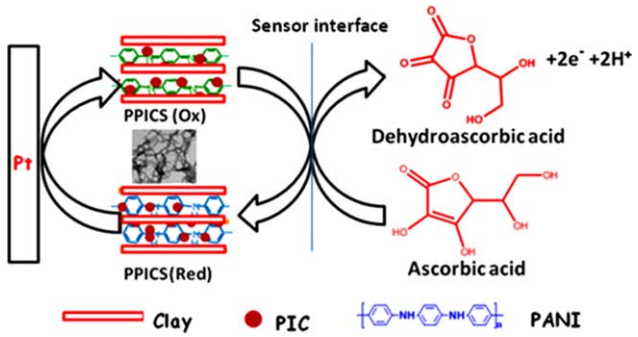

Scheme 2. Sequence of events that occur in a PPICS–mediated AA sensor. [Color figure can be viewed in the online issue, which is available at wileyonlinelibrary.com.]

the voltammetric response of AA with PPICS/Pt confirmed the sensitivity of AA. The increase in the current density was also enhanced by the transportation of electrons between Pt and AA mediated by the conductive magnetic PPICS.

Experiments were performed with increasing concentrations of AA. The cyclic voltammograms are given in Figure S8 (Supporting Information). We checked the linearity of the voltammetric response of AA by plotting the current against the concentration (7–40 n*M*), as shown in Figure 4; this gave a straight line with a correlation coefficient of 0.998. The lower detection limit was found to be 0.1 n*M*. Comparative details showing the better detection limit of this sensor with the literature reports are given in the Supporting Information (Table S1). This sensor could detect AA at nanomolar level compared to the micromolar detection observed with modifiers such as PANI, metal nanoparticles, multiwalled carbon nanotubes, aminophenol, and poly(Nile Blue).[57–64] The enhancement in the voltammetric response observed at higher concentration of AA was due to the diffusion of radicals to the PPICS surface, which was in electronic communication with the Pt electrode. The higher detection limit exhibited by our system could be explained by the efficient catalytic activity the Fe^{3+}/Fe^{2+} couple present in the Keggin iron and also because of the favorable electrostatic attraction between the cationic PPICS and anionic AA.

The effect of v on I_p was investigated in the range 20–200 mV/s. The plot of the dependence of the catalytic I_p on the square

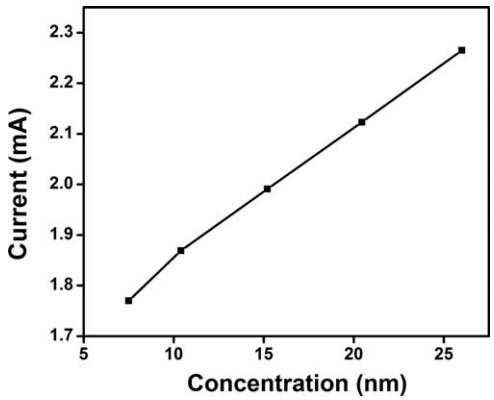

Figure 4. Variation in the current intensity as a function of the concentration of AA at the PPICS/Pt electrode in PBS (pH = 7).

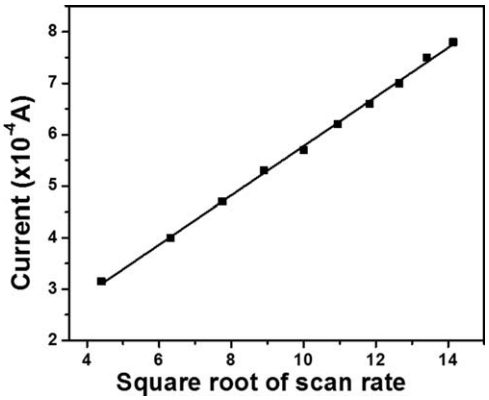

Figure 5. Plot of the dependence of the catalytic I_p's on the square root of the scan rates.

root of the scan rates showed linearity with a correlation coefficient of 0.965 and is shown in Figure 5.

According to Fick's law, we concluded this system to be a diffusion-controlled one rather than a surface-reaction process.[65] Theoretically, the electrochemical reaction of the analyte at the CP is complex and is associated with three processes:

1. Diffusion of the analyte to the CP.
2. Reaction between the CP and the analyte.
3. Transfer of the charge within the CP.

If the combination of relative rates of 2 and 3 exceeds the rate of 1, the electrochemical reaction occurs at the analyte–CP interface and is a diffusion-controlled process. This will result in the acceleration of the current intensity at a relatively low overvoltage. We made the same observation, and this further substantiated that the reaction of AA at the PPICS/Pt interface was a diffusion-controlled process. The number of electron–proton transfers taking place in the aqueous PPICS/Pt electrode interface during AA oxidation was evaluated by plotting ΔE_p versus ln v; this is shown in Figure S9 (Supporting Information). The slope of the curve was measured as 22 mV; this indicated that the oxidation was a two-electron, two-proton transfer

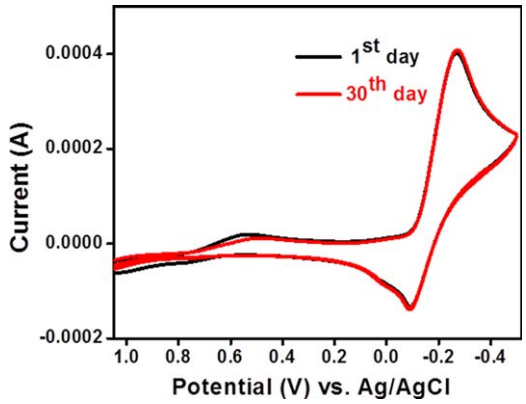

Figure 6. Cyclic voltammograms of PPICS for the first and last days of a month to demonstrate its excellent storage stability. [Color figure can be viewed in the online issue, which is available at wileyonlinelibrary.com.]

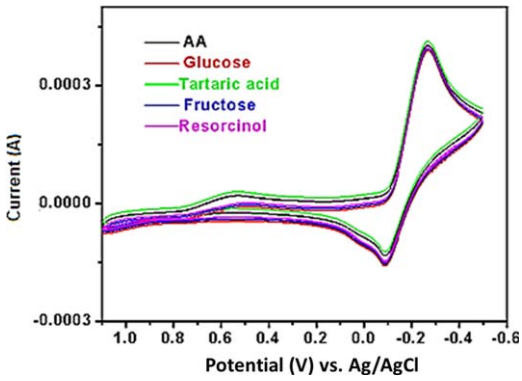

Figure 7. Effects of various possible interferences on the estimation of AA. [Color figure can be viewed in the online issue, which is available at wileyonlinelibrary.com.]

process.[66] The charge-transfer coefficient (α) and K_S^o were calculated to be $\alpha = 0.5$ and $K_S^o = 0.55\ s^{-1}$, respectively.

Sensitivity and Precision

We checked the sensitivity of the electrode by injecting a known amount of AA and back-calculating its concentration from the linear curve. Triplicate experiments were also performed to check the reproducibility of the results; these are shown in Figure S10 (Supporting Information). Sensitivity was observed with a minimum relative standard deviation of 1–2%. Such sensitivity was ascribed to the huge surface area, which loaded more AA and was advantageous to the transfer of the electron to the electrode. The response time was observed to be less than 15 s to reach steady state; this proved the high catalytic efficiency of the PPICS. In general, the nanostructured PPICS transduced and amplified the signal and increased the electrode's sensitivity to the AA assay.

Operational Stability and Shelf Life

The electrode current showed stability during the continuous scanning between potentials of 1 and −0.6 V for 50 cycles, as shown in Figure S11 (Supporting Information). This revealed that the electroactive species was highly active, and its activity did not decrease even after 50 cycles. Also when this modified electrode was swept in an AA solution for a long time, no pollution phenomenon was observed. Thus, it is promising to develop these sensors further because of their easy fabrication and stability.

The electrochemical storage stability (shelf life) of the PPICS electrode was a matter of investigation. We tested the reproducibility of the results by repeating the electrochemical process at various intervals of time within a month and comparing the intensity of the oxidation peak obtained with that of the initial stage. All of the trials resulted in the oxidation of AA at −0.32 V with the lowest decrease in the background current (Figure 6). These results substantiate the suitability of the PPICS-modified Pt electrode sensor for practical applications of the AA assay.

Interference Studies

To evaluate the selectivity of the PPICS/Pt sensor for AA, the effect of common potentially interfering compounds (organic acids, antioxidants, and sugars) on AA were investigated; the

Table I. Recovery of AA in the Presence of Some Possible Interference at the PPICS/Pt Electrode

Additive	Additive concentration (m*M*)	AA concentration (m*M*)	Current intensity (mA)		Signal recovery (%)
			Before addition	After addition	
Glucose	1	1	0.4	0.38	95
Fructose	1	1	0.4	0.385	96.3
Tartaric acid	1	1	0.4	0.4	100
Resorcinol	1	1	0.4	0.39	97.5

results are shown in Figure 7. Concentrations higher than those of the natural levels expected in food samples were tested by the measurement of the AA content of a 1 m*M* stock solution in the presence of the potential interferents, such as glucose, fructose, resorcinol, and tartaric acid. Table I summarizes the percentage signal recovery of the determination of 1 m*M* AA in the presence of millimolar concentrations of various interferences. The average signal recovery ranged from 95 to 100%; this indicated that the tested species did not cause much interference and, thereby, demonstrated the specificity and selectivity of the PPICS sensor to AA over many interfering compounds.

Analytical Application

The sensor activity was further validated by the quantitative determination of AA present in a vitamin C tablet. The vitamin C tablet was dissolved in PBS (pH 7.4), and the insoluble particles were removed by filtration. We recorded the CV response by repeating the analysis with a definite volume of analyte to the buffer. The cyclic voltammogram and the linear plot with a correlation coefficient of 0.997 was obtained and are given in Figure S12 (Supporting Information).

CONCLUSIONS

In conclusion, we prepared a water-dispersible PANI–Keggin iron–clay composite using a low-cost amphiphilic dopant, 3-PDPSA, derived from cashew nut shell liquid. This amphiphilic dopant controlled the size of the metal nanoparticles by preventing them from agglomerating and could also act as a micellar template for the formation of nanostructured PANI. These nanotapes exhibited an electrical conductivity of 100 S/m, an M_S of about 1 emu/g, and thermal stability above 350°C. Furthermore, we demonstrated the design of the PPICS-modified Pt electrode as an electrochemical sensor for the assay of AA. The lower detection limit for AA was observed at 0.1 nm. Lower noise, better stability, good reproducibility, and a fast response time open wide possibilities for the use of this electrode in the field of sensors. The electrode exhibited excellent sensitivity, good selectivity, and antifouling properties. All of these results suggest that the aqueous PPICS/Pt electrode could serve as a prospective low-cost and efficient electrochemical sensor and can provide promising and outstanding contributions to the food, beverage, and medical industries.

ACKNOWLEDGMENTS

The authors thank the Council of Scientific and Industrial Research (New Delhi, India)–MULTIFUN (Multifunctional electrode and electrolyte for future Technologies) Programme CSC 0101 for its financial support. They also thank Suresh Das, Director, National Institute for Interdisciplinary Science and Technology (NIIST), Trivandrum and A. Ajayaghosh, NIIST, Trivandrum, for their constant encouragement and support. They are also thankful to P. Guruswamy, M. Chandran, and Robert Philip for XRD, scanning electron microscopy, and TEM.

REFERENCES

1. Huang, J.; Virji, S.; Weiller, B. H.; Kaner, R. B. *Chem.—Eur. J.* **2004**, *10*, 1314.
2. Hatchett, D. W.; Josowicz, M. *Chem. Rev.* **2008**, *108*, 746.
3. Boroumand, F. A.; Fry, P. W.; Lidzey, D. G. *Nano Lett.* **2005**, *5*, 67.
4. Roman, L. S.; Inganäs, O.; Granlund, T.; Nyberg, T.; Svensson, M.; Andersson, M. R.; Hummelen, J. C. *Adv. Mater.* **2000**, *12*, 189.
5. Wang, J.; Chan, S.; Carlson, R. R.; Luo, Y.; Ge, G.; Ries, R. S.; Heath, J. R.; Tseng, H.-R. *Nano Lett.* **2004**, *4*, 1693.
6. Dong, B.; Lu, N.; Zelsmann, M.; Kehagias, N.; Fuchs, H.; Sotomayor Torres, C. M.; Chi, L. F. *Adv. Funct. Mater.* **2006**, *16*, 1937.
7. Eftekhari, A. Nanostructured Conductive Polymers; Wiley: Hoboken, NJ, **2011**.
8. Krutovertsev, S. A.; Sorokin, S. I.; Zorin, A. V.; Letuchy, Y. A.; Antonova, O. Y. *Sens. Actuators B* **1992**, *7*, 492.
9. Saumya, V.; Prathish, K. P.; Rao, T. P. *Talanta* **2011**, *85*, 1056.
10. Li, X. G.; Lu, Q. F.; Huang, M. R. *Small* **2008**, *4*, 1201.
11. Li, X. G.; Li, A.; Huang, M. R. *Chem.—Eur. J.* **2008**, *14*, 10309.
12. Li, X. G.; Feng, H.; Gu, G. L.; Moloney, M. G. *Anal. Chem.* **2012**, *84*, 134.
13. Huang, M. R.; Ding, Y. B.; Li, X. G. *Analyst* **2013**, *138*, 3820.
14. Li, X. G.; Huang, M. R.; Duan, W.; Yang, Y. L. *Chem. Rev.* **2002**, *102*, 2925.
15. Mitchell, I. V.; Purnell, J. H. Pillared Layered Structures: Current Trends and Applications; Elsevier Applied Science: New York, **1990**.
16. Mitchell, I. V.; Atkins, M. P. Pillared Layered Structures: Current Trends and Applications; Elsevier Applied Science: New York, **1990**.

17. Bradley, S. M.; Kydd, R. A. *J. Chem. Soc. Dalton Trans.* 1993, 2407. DOI: 10.1039/DT9930002407.
18. Ksenofontov, V.; Gaspar, A. B.; Niel, V.; Reiman, S.; Real, J. A.; Gütlich, P. *Chem.—Eur. J.* **2004**, *10*, 1291.
19. Reena, V. L.; Pavithran, C.; Verma, V.; Sudha, J. D. *J. Phys. Chem. B* **2010**, *114*, 2578.
20. Reddy, K. R.; Lee, K.-P.; Gopalan, A. I. *J. Appl. Polym. Sci.* **2007**, *106*, 1181.
21. Hiemenz, P. C. Principles of Colloid and Surface Chemistry; Marcel Dekker: New York, **1986**.
22. Sudha, J. D.; Sasikala, T. S. *Polymer* **2007**, *48*, 338.
23. Sudha, J. D.; Reena, V. L.; Pavithran, C. *J. Polym. Sci. Part B: Polym. Phys.* **2007**, *45*, 2664.
24. Sudha, J. D.; Reena, V. L. *Macromol. Symp.* **2007**, *254*, 274.
25. Reena, V. L.; Sudha, J. D.; Pavithran, C. *J. Appl. Polym. Sci.* **2009**, *113*, 4066.
26. Reena, V. L.; Sudha, J. D.; Ramakrishnan, R. *J. Appl. Polym. Sci.* **2013**, *128*, 1756.
27. Dumas, M.; Chaudagne, C.; Bonte, F.; Meybeck, A. C. R. *Acad. Sci. Ser. III* **1996**, *319*, 1127.
28. Aoki, A.; Matsue, T.; Uchida, I. *Anal. Chem.* **1992**, *64*, 44.
29. Uchiyama, S. *Talanta* **1992**, *39*, 1289.
30. Matos, R. C.; Augelli, M. A.; Pedrotti, J. J.; Lago, C. L.; Angnes, L. *Electroanal.* **1998**, *10*, 887.
31. Makower, A.; Eremenko, A. V.; Streffer, K.; Wollenberger, U.; Scheller, F. W. *J. Chem. Technol. Biotechnol.* **1996**, *65*, 39.
32. Wheeler, B. L.; Caple, G.; Henderson, A.; Francis, J.; Cantrell, K.; Vogel, S.; Grey, S.; Russell, D. *J. Electrochem. Soc.* **1989**, *136*, 2769.
33. Kang, Y.; Lee, M.-H.; Rhee, S. B. *Synth. Met.* **1992**, *52*, 319.
34. Chang, S. C.; Rawson, K.; McNeil, C. *J. Biosens. Bioelectron.* **2002**, *17*, 1015.
35. Lakshmi, D.; Sharma, P. S.; Prasad, B. B. *Biosens. Bioelectron.* **2007**, *22*, 3302.
36. Bae, Z.-U.; Park, J.-H.; Lee, S.-H.; Chang, H.-Y. *J. Electroanal. Chem.* **1999**, *468*, 85.
37. Zhang, L.; Wan, M. *Adv. Funct. Mater.* **2003**, *13*, 815.
38. Hassan, P. A.; Sawant, S. N.; Bagkar, N. C.; Yakhmi, J. V. *Langmuir* **2004**, *20*, 4874.
39. Murphy, P. J.; Posner, A. M.; Quirk, J. P. *J. Colloid Interface Sci.* **1975**, *52*, 229.
40. Chen, S.-A.; Lee, H.-T. *Macromolecules* **1995**, *28*, 2858.
41. Tang, J.; Jing, X.; Wang, B.; Wang, F. *Synth. Met.* **1988**, *24*, 231.
42. Li, X.-G.; Lü, Q.-F.; Huang, M.-R. *Chem.—Eur. J.* **2006**, *12*, 1349.
43. MacDiarmid, A. G.; Epstein, A. *J. Synth. Met.* **1995**, *69*, 85.
44. Cao, Y.; Li, S.; Xue, Z.; Guo, D. *Synth. Met.* **1986**, *16*, 305.
45. Schwertmann, U.; Cornell, R. M. Iron Oxides in the Laboratory: Preparation and Characterization; Wiley: Hoboken, NJ, **2008**.
46. Neoh, K. G.; Pun, M. Y.; Kang, E. T.; Tan, K. L. *Synth. Met.* **1995**, *73*, 209.
47. Tandon, R. P.; Tripathy, M. R.; Arora, A. K.; Hotchandani, S. *Sens. Actuators B* **2006**, *114*, 768.
48. Rightor, E. G.; Tzou, M.-S.; Pinnavaia, T. J. *J. Catal.* **1991**, *130*, 29.
49. Long, Y.; Chen, Z.; Duvail, J. L.; Zhang, Z.; Wan, M. *Phys. B: Condens. Matter* **2005**, *370*, 121.
50. Nguyen, M. T.; Diaz, A. F. *Adv. Mater.* **1994**, *6*, 858.
51. Bidan, G.; Jarjayes, O.; Fruchart, J. M.; Hannecart, E. *Adv. Mater.* **1994**, *6*, 152.
52. Pruneanu, S.; Veress, E.; Marian, I.; Oniciu, L. *J. Mater. Sci.* **1999**, *34*, 2733.
53. Nalini, B.; Sriman Narayanan, S. *Anal. Chim. Acta* **2000**, *405*, 93.
54. Xu, J.-J.; Zhou, D.-M.; Chen, H.-Y. *Electroanalysis* **1998**, *10*, 713.
55. Kumar, S. A.; Chen, S.-M. *J. Mol. Catal. A* **2007**, *278*, 244.
56. Park, S.-G.; Park, J.-E.; Cho, E.-I.; Hwang, J.-H.; Ohsaka, T. *Res. Chem. Intermed.* **2006**, *32*, 595.
57. Lin, K. L.; Yeh, P. Y.; Chen, S. *Int. J. Electrochem. Sci.* **2012**, *7*, 12752.
58. Civit, L.; Nassef, H. M.; Fragoso, A.; O'Sullivan, C. K. *J. Agric. Food Chem.* **2008**, *56*, 10452.
59. Chairam, S.; Sriraksa, W.; Amatatongchai, M.; Somsook, E. *Sensors* **2011**, *11*, 10166.
60. Kong, Y.; Shan, X.; Ma, J.; Chen, M.; Chen, Z. *Anal. Chim. Acta* **2014**, *809*, 54.
61. Liu, Y.; Su, Z.; Zhang, Y.; Chen, L.; Gu, T.; Huang, S.; Liu, Y.; Sun, L.; Xie, Q.; Yao, S. *J. Electroanal. Chem.* **2013**, *709*, 19.
62. Chauhan, N.; Narang, J.; Rawal, R.; Pundir, C. S. *Synth. Met.* **2011**, *161*, 2427.
63. Huang, T. C.; Yeh, L. C.; Huang, H. Y.; Nian, Z. Y.; Yeh, Y. C.; Chou, Y. C.; Ming, J. *Polym. Chem.* **2014**, *5*, 630.
64. Kul, D.; Ghica, M. E.; Pauliukaite, R.; Brett Christopher, M. A. *Talanta* **2013**, *111*, 76.
65. Zakharchuk, N. F.; Meyer, B.; Henning, H.; Scholz, F.; Jaworksi, A.; Stojek, Z. *J. Electroanal. Chem.* **1995**, *398*, 23.
66. Castro, S. S. L.; Balbo, V. R.; Barbeira, P. J. S.; Stradiotto, N. R. *Talanta* **2001**, *55*, 249.